frontiers | Frontiers in Materials

TYPE Original Research
PUBLISHED 14 April 2023
DOI 10.3389/fmats.2023.1159444

OPEN ACCESS

EDITED BY
Luca Valentini,
University of Perugia, Italy

REVIEWED BY
Mario Fabiilli,
University of Michigan, United States
Gabriele Maria Fortunato,
University of Pisa, Italy

*CORRESPONDENCE
Eli Vlaisavljevich,
eliv@vt.edu

RECEIVED 05 February 2023
ACCEPTED 03 April 2023
PUBLISHED 14 April 2023

CITATION
Meyers KM, Simon A, Khan ZM, Rajachar RM and Vlaisavljevich E (2023), Focused ultrasound for the remote modulation of nitric oxide release from injectable PEG-fibrinogen hydrogels for tendon repair.
Front. Mater. 10:1159444.
doi: 10.3389/fmats.2023.1159444

Focused ultrasound for the remote modulation of nitric oxide release from injectable PEG-fibrinogen hydrogels for tendon repair

Kaylee M. Meyers[1], Alex Simon[2], Zerin M. Khan[2], Rupak M. Rajachar[1] and Eli Vlaisavljevich[2]*

[1]Department of Biomedical Engineering, Michigan Technological University, Houghton, MI, United States, [2]Department of Biomedical Engineering and Mechanics, Virginia Polytechnic Institute and State University, Blacksburg, VA, United States

Introduction: Tendon disorders such as tendinosis, the degradation of collagen in tendon, or tendonitis, inflammation of tendon tissue, contribute to 30% of musculoskeletal complaints. To address the limitations of currently available treatments for tendon repair, an injectable polyethylene glycol (PEG)-fibrinogen hydrogel encompassing nitric oxide (NO) releasing μ-particles was generated. The release of nitric oxide, a therapeutic molecule that modulates many wound healing processes, from the hydrogel can be modified with thermal and mechanical stimulus. To achieve remote control over NO release from hydrogels after deployment, focused ultrasound (FUS) was explored as it provides highly controlled thermal and mechanical stimulus non-invasively.

Methods: In this work, the ability of FUS to remotely elicit on-demand NO generation from acoustically active composite hydrogels via thermal and/or mechanical stimulus was explored. Specifically, the temperature and time-dependent release of NO was simulated and characterized when applying FUS to composite hydrogels.

Results: Results from acoustic simulations as well as thermocouple heating studies indicated that high spatial and temporal control over hydrogel warming could be achieved non-invasively with a 3.5 MHz FUS transducer. FUS was also able to remotely control NO release from hydrogels with various thermal magnitudes and durations. Additionally, no apparent changes in the mechanical properties of hydrogels were observed with FUS treatment.

Discussion: Utilizing FUS thermal and mechanical stimulus provides a potential method of remotely controlling NO release from hydrogels at a wound site to aid in tendon repair.

KEYWORDS

nitric oxide, composite hydrogels, tendon repair, focused ultrasound (FUS), stimuli-responsive

1 Introduction

Tendon injuries are typically the result of excessive tissue overloading, which can affect normal tendon architecture through the uncontrolled degradation and/or synthesis of the extracellular matrix (ECM). Currently, acute and chronic tendon injuries are treated with moderately effective reconstructive surgeries and corticosteroid injections (Nourissat et al., 2015). As an alternative or complementary approach to accelerating repair in tendon tissue, an injectable, adhesive polyethylene glycol (PEG)-fibrinogen based hydrogel containing S-Nitroso-N-acetyl penicillamine (SNAP)-fibrin μ-particles was previously developed (Joseph et al., 2019). With the inclusion of SNAP, a nitric oxide donor, in μ-particles, the composite hydrogel had the capacity to release controlled amounts of nitric oxide (NO) in response to thermal and mechanical stimulation (VanWagner et al., 2013; Joseph et al., 2019).

NO is a reactive nitrogen species that acts as an antimicrobial signaling molecule and is involved in multiple wound healing cascades and immunoregulation (Bogdan et al., 2000; Garcia-Ortiz and Serrador, 2018). Additionally, endogenous NO has been shown to modulate the production of various cytokines, chemokines, and growth factors that aid in tissue regeneration (Bogdan, 2001; Guzik et al., 2003). The antimicrobial properties of NO are a result of the reaction between NO and superoxide which leads to the formation of peroxynitrite, a highly oxidative species that damages bacterial proteins (Kim et al., 2015). NO also plays a role in maintaining the dynamic equilibrium of protein deposition and degradation that occurs during ECM homeostasis via the transcriptional and post-transcriptional regulation of matrix degrading proteases, specifically matrix metalloproteinases (MMPs) (Chakrabarti and Patel, 2005). The modulation of ECM turnover enables the prevention of excessive degradation and/or deposition of matrix which can lead to the formation of mechanically weakened and/or stiff fibrotic-like matrix. Controlling the balance in ECM degradation and deposition could help accelerate wound healing processes since changes in the physical properties of the ECM can influence cell decisions and fate through biomechanical signaling (Watt and Hogan, 2000; Vogel and Sheetz, 2006; Halder et al., 2012; Trappmann et al., 2012). Previous work has shown that the thermally controlled release of NO from our SNAP-fibrin μ-particles can both activate and inhibit MMP activation in a time and dose-dependent manner (data not yet published).

Despite the many beneficial effects of NO, its presentation at an injury site in excessive amounts can be detrimental to the local wound healing environment via oxidative damage and chronic inflammation (Dunnill et al., 2017; de Vries et al., 2020). This necessitated the development of a system for the remote-controlled delivery of exogenous NO from the injectable composite hydrogels. Focused ultrasound (FUS) has gained increased recognition for clinical applications in tissue heating, tumor ablation, and drug-delivery as it is a non-invasive therapy that provides highly precise spatial and temporal control during treatment (Zhou, 2011; ter Haar, 2015). Specifically, the employment of thermal and/or mechanical stimuli from FUS have been used in targeted drug delivery in combination with artificial agents such as gas-filled microbubbles, fluid-filled nanoparticles, and gas-stabilizing solid nanocups (Burgess et al., 2018; Khirallah et al., 2019; Rehman et al., 2019; Yildirim et al., 2019; Lapin et al., 2020). In addition, acoustically active scaffolds have been designed to generate on-demand controlled release of therapeutics (Moncion et al., 2016). The utilization of FUS in the delivery of drugs has many advantages including the ability of FUS waves to induce convection of the delivered therapeutic molecule at the targeted area, cause the perturbation or degradation of the therapeutic carrier to increase the release of the desired drug, and potentially increase both tissue and cell permeability and diffusivity to augment the effectiveness of therapeutics (Pitt et al., 2004). Since FUS provides a non-invasive method to controllably apply thermal and mechanical stimuli used to remotely elicit the controlled release of NO from our composite hydrogels, we hypothesized that FUS could be used with our injectable hydrogel system to remotely elicit exogenous NO release with high spatial and temporal control. Modulating exogenous NO dosages from the hydrogels could aid in regulating matrix synthesis/degradation and antimicrobial defense during the reestablishment of tissue structure and function in addition to the composite's passive functions of providing a provisional microenvironment for native or exogenous cells to adhere, infiltrate, and remodel (Figure 1). This interdisciplinary approach to tendon repair aims to bridge the gap between the development of regenerative biomaterials and their clinical applications for targeted drug delivery with the use of FUS.

To evaluate the potential of FUS to elicit thermally and/or mechanically induced NO release from SNAP-fibrin μ-particles incorporated in PEG-fibrinogen hydrogels, first a FUS system was fabricated with a 3.5 MHz transducer, a custom-built positioning system, and 3D printed ultrasonically conductive sample holders. Next, a simulation was conducted to characterize and map the acoustic pressure near the focal region of the FUS transducer under a range of exposure parameters. Thermocouples were then utilized to quantify the thermal effects of different FUS treatment parameters (i.e., duty cycle, duration, and driving voltage) on composite hydrogels. A nitric oxide analyzer was then used with the FUS system to evaluate the real-time release of NO from composite hydrogels in response to FUS stimulus. Finally, the mechanical properties of hydrogels treated with FUS were determined with compression and rheometric testing to assess for FUS mediated damage.

2 Materials and methods

2.1 SNAP-fibrin and fibrin μ-particle synthesis

Previously published work highlights the synthesis and characterization (e.g., particle size, composition analysis, *etc.*) of SNAP-fibrin μ-particles in detail (VanWagner et al., 2013; Joseph et al., 2019). Briefly, particles were generated via inverse emulsions in olive oil with an overhead stirrer (Fisher Scientific D25; Waltham, MA) and a Teflon impeller (Fisher Scientific, Waltham, MA). For SNAP-fibrin μ-particles, SNAP crystals were first produced by sonicating N-acetyl-D-penicillamine (NAP; Sigma Aldrich, St. Louis, MO) (100 mg) in methanol. Once dissolved, hydrochloric acid (15 mL), sulfuric acid (500 μL), and sodium nitrite (724.5 mg) was added to this solution. After the solution reacted for 1 h, methanol was removed by rotary evaporation. SNAP crystals were cooled and then isolated by vacuum filtration. To synthesize

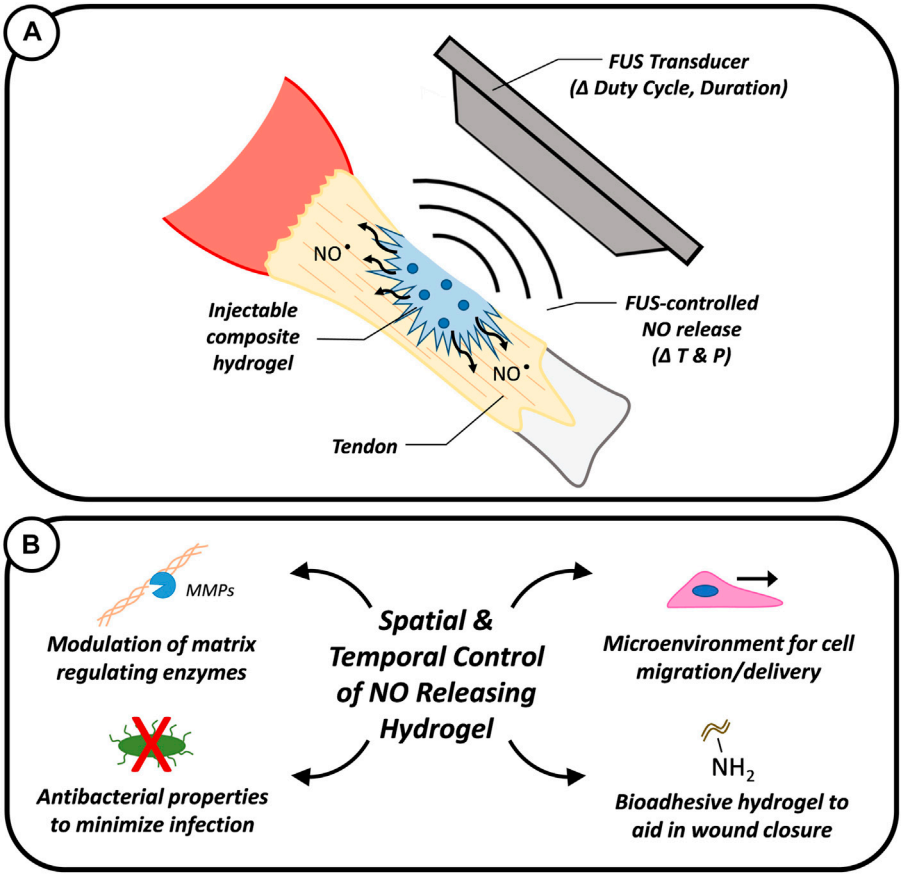

FIGURE 1
Graphic showing the intended use of FUS to remotely modulate the release of NO from composite hydrogels to aid in tendon repair via controlled temperature (T) and pressure (P) stimulus **(A)**. The spatial and temporal controlled release of NO could enable the modulation of matrix regulating enzymes and the minimization of bacterial infections while the composite hydrogel could provide a physical microenvironment to support cell adhesion and migration **(B)**.

SNAP-fibrin μ-particles, SNAP crystals (20 mg) were dissolved in phosphate buffered saline (PBS; 1.8 mL) with sodium hydroxide and hydrochloric acid. After fibrinogen (200 mg) was dissolved in the solution, it was added dropwise to the inverse emulsion. To crosslink the droplets, thrombin (50 units) and calcium chloride (3 mg) dissolved in PBS (0.5 mL), was added to the flask. Particles were isolated via vacuum filtration, rinsed with chilled acetone, vacuum dried for 1 h, and stored at 4°C for later use. Fibrin only μ-particles were generated similarly but without the addition of the SNAP crystals.

2.2 Composite hydrogel synthesis

For all experiments involving the synthesis of composite PEG-fibrinogen hydrogels, protocols outlined in previously published work focused on composite hydrogel formulation and characterization (e.g., hydrogel composition analysis and mechanical property testing) were followed (Joseph et al., 2019). Briefly, four-arm polyethylene glycol succinimidyl glutarate (JenKem, Plano, TX) (67 mg/mL) was dissolved in PBS (pH 7.4) with fibrin μ-particles, SNAP-fibrin μ-particles, or no addition of μ-particles. To polymerize PEG-fibrinogen gels, equal volumes of fibrinogen from bovine plasma (Sigma Aldrich, St. Louis, MO) (134 mg/mL) dissolved in PBS and PEG-NHS solution were mixed and allowed to fully cure for 30 min at room temperature.

2.3 FUS system experimental set-up

For FUS studies, a 3.5 MHz transducer (SU-107; Sonic Concepts, Bothell, WA) with a f-number of 8.8 was driven by a function generator (ValueTronics, Elgin, IL) and radiofrequency power amplifier (240L; Electronics & Innovation, Ltd., Rochester, NY) were utilized to treat samples submerged in a tank of degassed water (Figure 2). Custom water-tight sample holders designed with wells 12.5 mm in diameter and 8 mm in depth (Inventor Professional 2019; Autodesk, San Rafael, CA) were 3D printed (Form3 Basic 3D printer; Formlabs, Somerville, MA) with an ultrasonically conductive resin (Elastic Resin, Formlabs). Wells contained 800 μL of formulated hydrogel and remaining well volume was filled with water. Targeting of samples was achieved using a custom 3D positioning system driven with a MATLAB program. The temperature of samples treated with FUS were monitored with Type T needle thermocouples (Physitemp Instruments, Clifton, NJ) and data

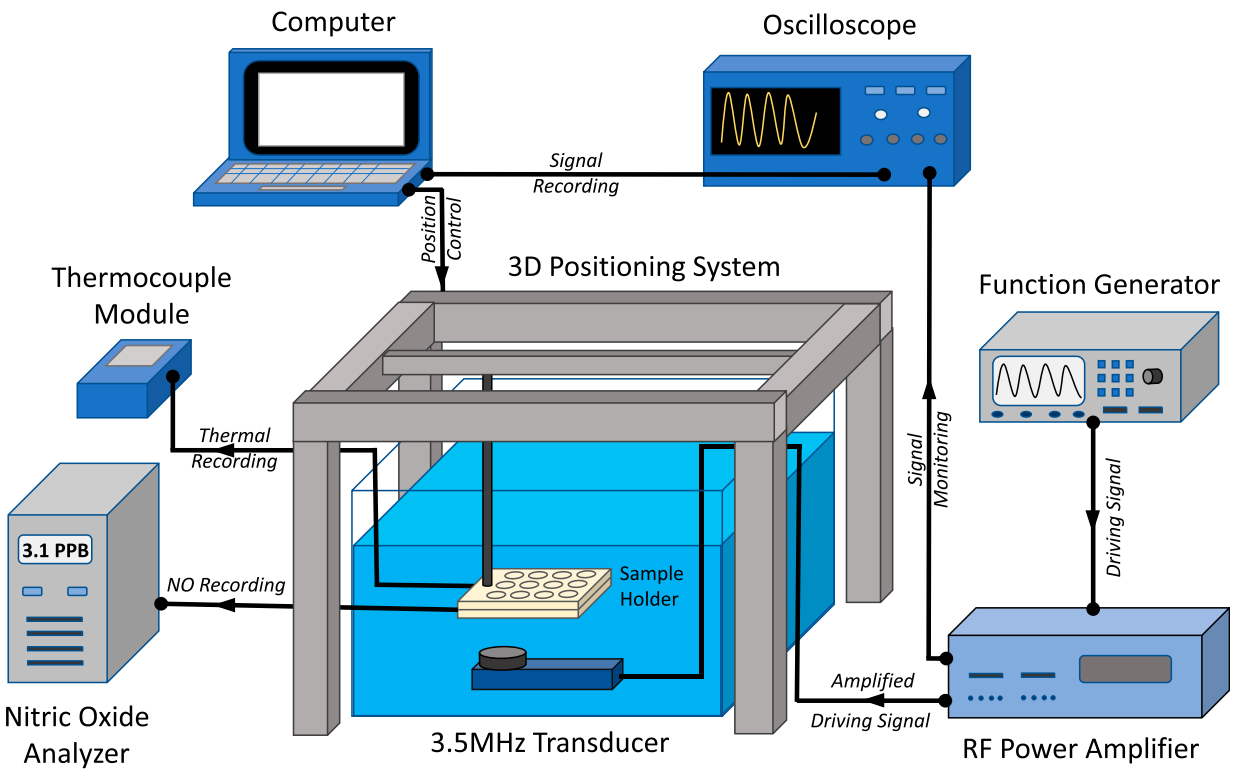

FIGURE 2
Schematic showing experimental set-up of FUS system. The transducer was driven by a function generator and radio frequency (RF) power amplifier. Driving signals were monitored with an oscilloscope and a 3D positioning system was used to align the FUS transducer focal region in sample holders. Thermocouples were utilized to monitor sample temperature while a nitric oxide analyzer was used to record NO release.

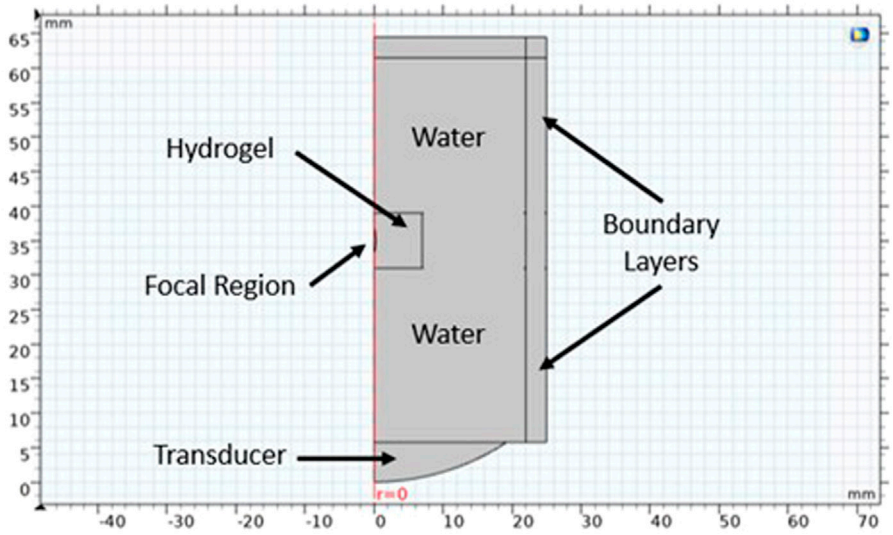

FIGURE 3
2D axisymmetric geometry used to model FUS treatment of the hydrogel in a water bath.

TABLE 1 Acoustic, thermal, and mechanical properties of water and a PEG-based hydrogel.

Material	Water	Hydrogel
Density (kg/m^3)	1,000	1,010
Speed of Sound (m/s)	1,483	1,520
Attenuation (Np/m/MHz)	0.025	0.4

logger (Omega Engineering, Norwalk, CT). A Sievers 280i nitric oxide analyzer (NOA; Boulder, CO) was used to measure real-time NO release.

2.4 Finite element analysis acoustics simulations

To simulate acoustic propagation in hydrogels treated with FUS, a geometry was first modeled and meshed, whereafter appropriate material assignment and boundary conditions were applied to the model as described below. Methods from COMSOL Multiphysics tutorials on simulations of FUS treatment of tissue phantoms were utilized in this study (Focused Ultrasound Induced Heating in Tissue Phantom, 1265). FUS stimulation of the hydrogel in a water bath was simulated with acoustics functions in COMSOL Multiphysics software (Version 5.4; COMSOL Incorporated, Stockholm, Sweden). The two-dimensional axisymmetric geometry of a focused ultrasound transducer with a 0.46 mm × 3.5 mm ellipse focal region consistent with the transducer manufacturer's specifications (SU-107; Sonic Concepts) and a composite hydrogel in a water bath were generated in COMSOL (Figure 3). Boundary layers were assigned near the geometric edges of the model to establish boundary conditions that attenuated pressure waves to prevent acoustic reflections from interfering with the simulations.

The acoustic, thermal, and mechanical properties of water and a PEG-based hydrogel were tabulated and assigned to appropriate regions in the geometry (Table 1). The exact acoustic and thermal properties of the composite hydrogel in this study were not experimentally measured but assumed to be similar to PEG-based hydrogels in the literature (Rice et al., 2009; Cabaleiro et al., 2020).

The acoustic simulation performed in this study utilized free triangular shaped elements. Element size for the simulations was finer near the focal region of the geometry to resolve the wavelength of the 3.5 MHz acoustic pressure waveforms. Specifically, the mesh element size in the focal region was 4.3 × 10^{-5} mm and 8.5 × 10^{-5} mm in the rest of the geometry. The stationary acoustic pressure field created by the transducer was modeled in the frequency domain by solving the homogeneous Helmholtz equation (1) (Focused Ultrasound Induced Heating in Tissue Phantom, 1265):

$$\frac{\partial}{\partial r}\left[\frac{-r}{\mathrm{r}_c}\left(\frac{\partial p}{\partial r}\right)\right] + r\frac{\partial}{\partial z}\left[\frac{-1}{\mathrm{r}_c}\left(\frac{\partial p}{\partial z}\right)\right] - \left[\left(\frac{\mathrm{w}}{c_c}\right)^2\right]\frac{rp}{\mathrm{r}_c} = 0 \qquad (1)$$

Where r and z are cylindrical coordinates of the geometry, p is acoustic pressure, w is angular frequency, r_c is the density of the material and c_c is speed of sound through the material.

2.5 Acoustic pressure measurements

The acoustic output at the focal region of the 3.5 MHz FUS transducer was measured using a rod hydrophone (HNR-500; Onda Corporation, Sunnyvale, CA) over a range of various driving voltages (1–20 V) with a pulse repetition frequency of 50 Hz. Pressure waveforms and driving voltage measurements were recorded for FUS pulses applied with 1, 5, 10, 15, and 20 cycles using an oscilloscope and graphed with MATLAB.

2.6 FUS heating of hydrogels

The focal point of the transducer was located with a custom stereotactic device and placed directly in the center of each well in the sample holder for targeting with the positioning system. Sample holders containing PEG-fibrinogen (PF), PEG-fibrinogen with 4.8 mg of fibrin microparticles (F), and PEG-fibrinogen with 4.8 mg of SNAP-fibrin microparticles (SF) hydrogel formulations were treated with continuous wave FUS using the 3.5 MHz transducer. The driving voltage of the system was varied to heat and maintain the desired temperature within the hydrogels. Specifically, continuous sinusoidal waveforms with peak acoustic pressures of ±5.8 MPa and +3 MPa were utilized to warm and maintain the hydrogel at 42°C. Thermocouples were used to monitor the temperature of hydrogels throughout the duration of each FUS treatment.

2.7 Thermal nitric oxide release quantification

The release of nitric oxide from PEG-fibrinogen hydrogels containing 2.4, 4.8, and 8.1 mg of SNAP-fibrin microparticles (SF) in response to FUS treatment was directly determined in real-time with a nitric oxide analyzer. NO release curves were analyzed with a custom MATLAB program as described in prior studies (He and Frost, 2016a; He and Frost, 2016b).

2.8 Mechanical characterization of FUS treated hydrogels

To evaluate hydrogel stiffness with and without FUS heating treatment, a custom-built micro-indentation device consisting of a 10 g load cell (Transducer Techniques), high resolution miniature linear stage stepper motor (MFA-PPD, Newport), and an indenter (ALS-06, Transducer Techniquesand) was utilized (Narkar et al., 2019). Stiffness was quantified as the average slope of indenter contact area (mm^2) *versus* compressive force (N) near the measurement of maximum compressive force.

Rheometric characterization was performed on hydrogels containing 4.8 mg of SNAP-fibrin particles with and without FUS heating treatment to quantify viscoelastic behavior. A rheometer (TA Instruments; Newcastle, DE) with a parallel plate diameter of 20 mm was used to carry out frequency sweep experiments (between 0.1 and 40 Hz) to determine storage modulus (G′) and loss modulus

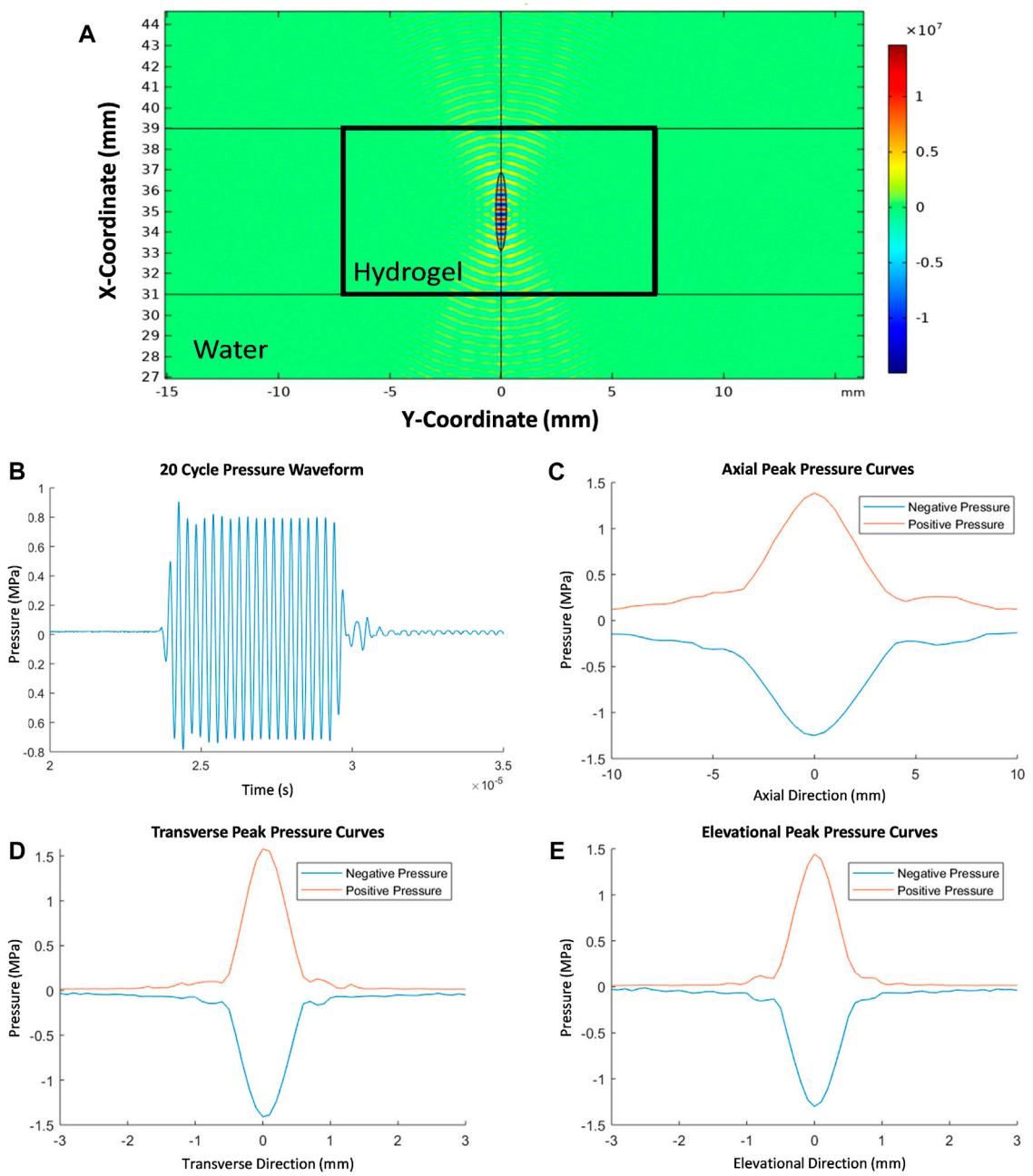

FIGURE 4
FEA simulation of 2D acoustic pressure field (Pa) showing the stationary acoustic pressure generated in the FUS focal region encompassed by the composite hydrogel **(A)**. Representative pressure waveform measured at the focus of the FUS transducer when driven at 20 cycles per burst **(B)**. Linear scans of the pressure in the focal region in axial, transvers, and elevational directions **(C–E)**.

(G″). Samples were evaluated at 10% strain in compression and 1% strain in shear.

2.9 Statistical analyses

All statistical analyses were made using Tukey's HSD tests with JMP software (Cary, NC) where p-values less than 0.05 ($p < 0.05$) were considered significant. Error bars represent standard deviation.

3 Results and discussion

3.1 FUS transducer acoustics characterization

Simulation results for the acoustic pressure field generated by the FUS transducer in the hydrogel showed that ±15 MPa of pressure (30 MPa peak-to-peak) was generated in the focal region with negligible pressure change in the surrounding water bath

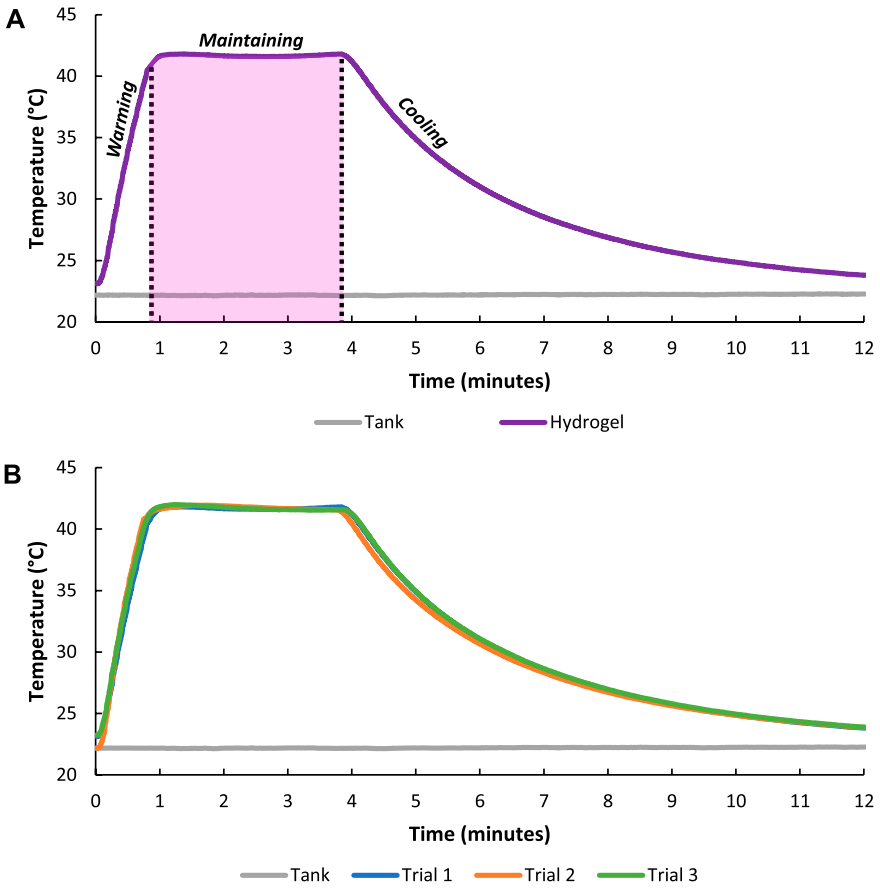

FIGURE 5
Temperature of the composite hydrogel during FUS warming (±5.8 MPa) to about 42°C, FUS treatment to maintain (±3 MPa) 42°C for 3 min, and cooling with FUS system turned off (0 MPa) **(A)**. FUS heating of composite hydrogel over three trials showing the repeatability of the treatment scheme **(B)**.

(Figure 4A). As expected, peak positive and negative pressures were observed near the 35 mm x-coordinate which is the target focal length of the transducer. The exact location of the peak pressures observed in the simulation appear to be slightly less than 35 mm (off by about 0.1 mm) due to the minor refractive effects of the hydrogel on the generated acoustic waves. However, the acoustic simulation did not account for the presence of microparticles or any effects of varying concentration of microparticles on acoustic attenuation of the composite hydrogels. Existing literature suggests that microparticle presence and increasing concentrations in the composite hydrogel would increase acoustic attenuation (Drakos et al., 2021). Another limitation of the acoustic simulation when compared to experimental FUS treatments of the hydrogels was the absence of the potential effects of the hydrogel sample well holders on acoustic attenuation. Experimental pressure waveforms produced by the FUS transducer in water were recorded when driven at 20 cycles per burst (Figure 4B). Linear pressure scans were performed to map the ellipsoid focal region of the transducer (Figures 4C–E). Results indicated that the −6 dB focal region measured 4.0 mm in the axial direction and 0.5 mm in the transverse and elevational directions which was consistent with manufacturer specifications.

3.2 FUS heating of hydrogels

Continuous FUS stimulation was used to controllably heat composite hydrogels to 42°C and maintain the hydrogels at 42°C for 3 min whereafter FUS stimulus was removed and hydrogels were allowed to cool for 8 min (Figure 5A). Pressures of approximately ±5.8 MPa and ±3 MPa were generated during the hydrogel heating and maintenance periods, respectively, with the time required to warm the hydrogels to 42°C taking about 50 s. The spatial peak-temporal average intensities during hydrogel heating and maintenance periods were 1,100 W/cm^2 and 300 W/cm^2. A maintenance temperature of 42°C was utilized during FUS heating because 42°C is near the upper limit of therapeutic heating windows where thermal damage to surround tissues could be avoided during *in vivo* applications (Rao et al., 2010; Schildkopf et al., 2010; Behrouzkia et al., 2016). Minimal deviation from 42°C was observed during the FUS heating maintenance period, demonstrating that FUS stimulation provided a highly controlled means of non-invasively and continuously heating a targeted region within the hydrogel. The heating and cooling behavior of the hydrogels was fitted with exponential functions (3–4). Specifically, the warming curve was approximated with:

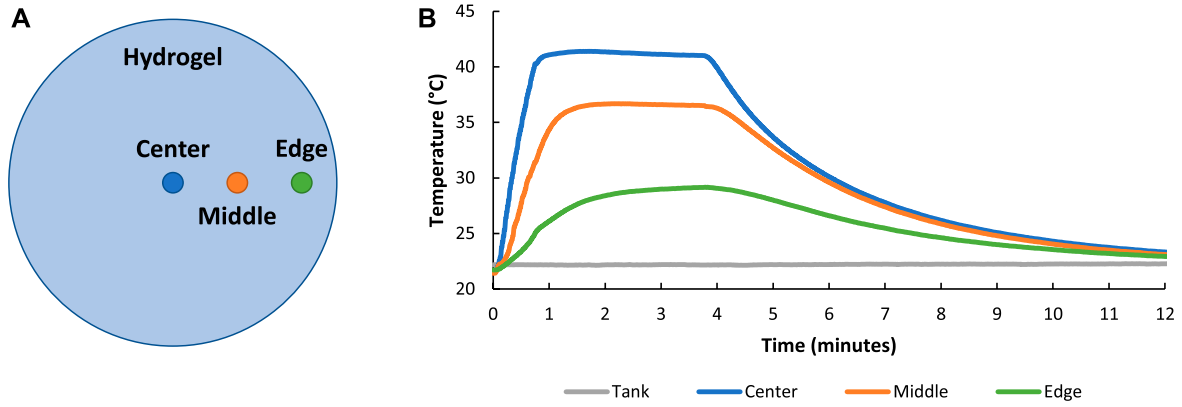

FIGURE 6
Image showing the location of thermocouples placed in the hydrogel to study thermal conduction of FUS treatment throughout the hydrogel volume **(A)**. FUS heating of composite hydrogel showed that heating was greater in the center of the hydrogel (nearest to the focal region of the transducer) when compared to the middle and edge of the hydrogel (further from the focal region of the transducer) **(B)**.

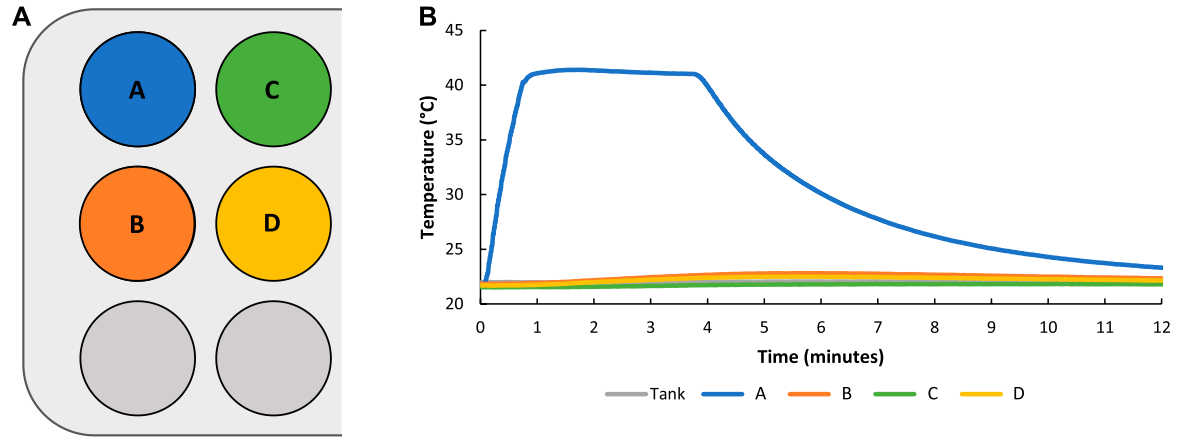

FIGURE 7
Graphic showing naming convention and location of hydrogels in sample holder wells with hydrogel A being targeted with FUS controlled heating **(A)**. During FUS targeted heating of sample A minimal heating of hydrogels in other sample holder wells (≤1°C) was observed showing tight spatial control of FUS heating **(B)**.

$$T = -0.1^{5.2t} + 22.1^{0.9t} \quad (2)$$

Where T is temperature in degrees Celsius and t is time in minutes (R^2 = 0.9969). The cooling curve was approximated with:

$$T = 13.5^{-0.5t} + 26.5^{-0.01t} \quad (3)$$

Where T is temperature in degrees Celsius and t is time in minutes (R^2 = 0.9997).

The repeatability of hydrogel heating was evaluated by running the FUS treatment regime over three different trials. Results showed minimal variation in hydrogel heating and cooling curves among trials indicating tight temporal and heating magnitude control with the FUS transducer (Figure 5B).

The conduction of heat through the hydrogel with applied FUS treatment was measured by inserting thermocouples in the center, middle (~3 mm from center), and edge (~6 mm from center) of the hydrogel (Figure 6A). As expected, hydrogel heating was greatest in the center of the hydrogel (42°C) near the focal region of the transducer and decreased when moving towards the edge of the hydrogel (27°C) further away from the focus of the transducer (Figure 6B).

The conduction of heat among hydrogels in the custom sample holders with applied FUS treatment was measured by inserting thermocouples in hydrogels located in adjacent wells surrounding a targeted FUS heated well (Figure 7A). Results indicated that adjacent hydrogels experienced minimal heating (≤1°C) throughout the duration of FUS treatment which showed tight spatial control of FUS heating (Figure 7B).

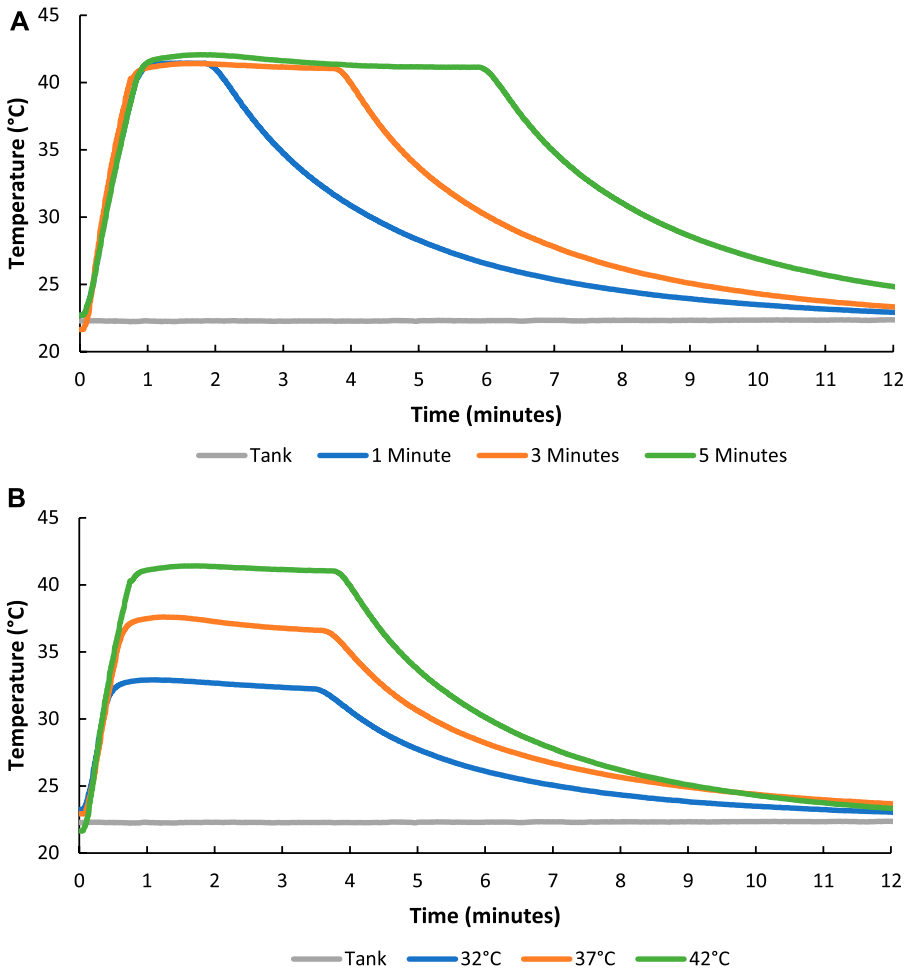

FIGURE 8
Graphs showing how the duration (1, 3, and 5 min of 42°C FUS maintenance) **(A)** and magnitude (32°C, 37°C, and 42°C) **(B)** of FUS heating treatment of the composite hydrogels could be tightly controlled.

The temporal control of FUS heating in hydrogels was evaluated by varying the duration of FUS treatment temperature maintenance periods for 1, 3, and 5 min (Figure 8A). Additionally, the ability to modulate the magnitude of FUS treatment was also tested by setting the transducer to maintenance temperatures at 32°C, 37°C, and 42°C (Figure 8B). Results from temperature duration and amplitude studies indicated that FUS heating of hydrogels could be modulated with tight temporal and magnitude control.

The rate of FUS controlled heating of hydrogels was also varied by altering the duty cycle of the transducer driving voltage signal (50, 70, and 100%) (Figure 9). As expected, when using relatively smaller duty cycles, the amount of time it took to reach 40°C was longer when compared to relatively higher duty cycles. More specifically, a 50% duty cycle took just under 3 min to warm a hydrogel to 40°C whereas a 70% and 100% duty cycle took roughly 1.5 min and 1 min respectively demonstrating control over the rate of hydrogel heating.

Different hydrogel compositions consisting of PEG-fibrinogen (PF), PEG-fibrinogen with fibrin microparticles (F), and PEG-fibrinogen with SNAP-fibrin microparticles (SF) hydrogels were heated to ~40°C (Figure 10). No differences in heating or cooling behavior among hydrogel formulations were observed, however "shoulders" on the maintain phase of the heating profile were noted, but this behavior may be a result of manually changing pulsing parameters on the driving instrumentation during the transition between FUS heating and maintenance treatments.

3.3 Controlled NO release from hydrogels with FUS

The real-time release of NO from hydrogels containing SNAP-fibrin particles in response to FUS treatment was evaluated with a nitric oxide analyzer. Hydrogels containing 4.8 mg of SNAP-fibrin particles were allowed to equilibrate for 30 min and then heated with FUS at 40°C for 5 min twice with a 45-min gap between treatments (Figure 11). NO release from FUS stimulated hydrogels showed instantaneous increases in NO with applied FUS heating. NO release continued to stay elevated until the hydrogels cooled back to baseline temperatures after about 10–15 min. Over the duration of the recording, overall NO release steadily increased which is consistent with baseline NO release curves from non-stimulated hydrogels. The rate of NO

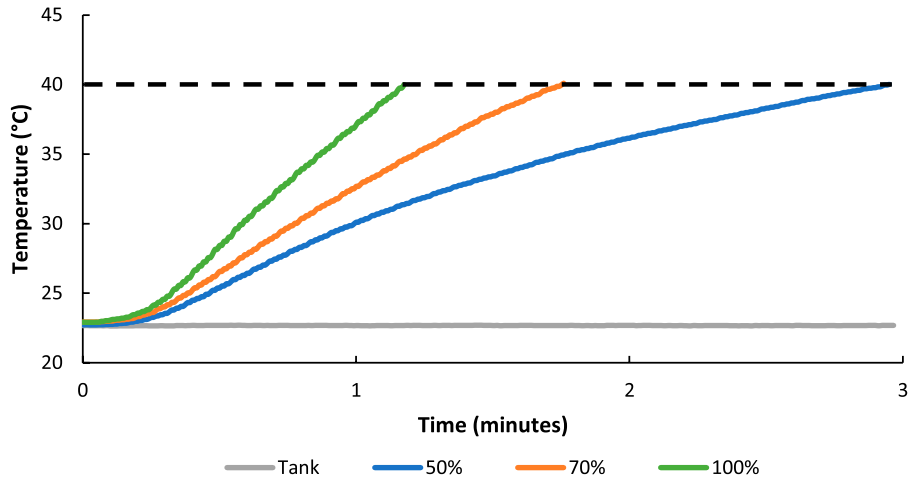

FIGURE 9
The rate of FUS controlled heating of hydrogels to 40°C was altered by setting the duty cycle of the driving signal to 50, 70, and 100% with the amplitude set constant at ±5.8 MPa.

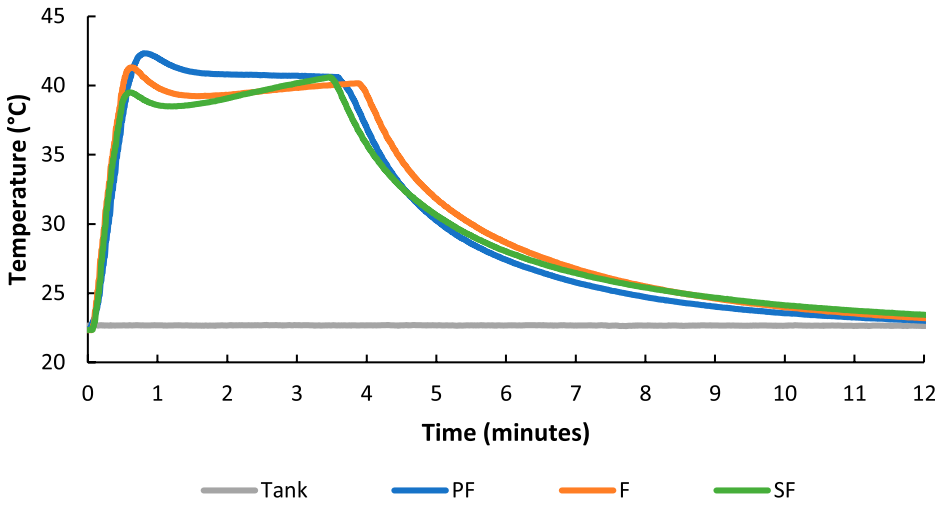

FIGURE 10
FUS heating of PEG-fibrinogen (PF), PEG-fibrinogen with fibrin microparticles (F), and PEG-fibrinogen with SNAP-fibrin microparticles (SF) hydrogel formulations showed no differences in heating character.

release was 0.18–0.21 PPB/minute during FUS induced warming of the hydrogels which was greater than the ~0.01 PPB/minute baseline NO release rate in the absence of FUS stimulus. Cumulative NO release over the 2-h recording with FUS treatments (2.30×10^{-9} mol NO) was higher when compared to non-stimulated hydrogels (1.41×10^{-9} mol NO). The difference in NO cumulative release between treated and untreated hydrogels was notable considering FUS stimulus was provided for only 8% of the duration of the recording. The thermal release of NO occurs via cleavage of the covalent S–N bond in SNAP within the microparticles of the composite hydrogel (VanWagner et al., 2013; Joseph et al., 2019). Non-thermal release of NO occurs from a number of different factors including mechanical, pH, and light stimuli (VanWagner et al., 2013; Joseph et al., 2019).

To assess the temporal control of FUS-mediated NO release, hydrogels were treated with 40°C and 60°C heating and cooling cycles. Spikes in NO release were achieved by stimulating the hydrogel to 40°C and allowing it cool for a total of 4 times (Figure 12A). Results showing distinct peaks in NO release indicated tight temporal control over NO presentation with FUS stimulation with peaks in NO release between about 1.4 and 1.6 PPB. Increasing the magnitude of heating to 60°C with FUS and allowing the hydrogel cool for a total of 4 times

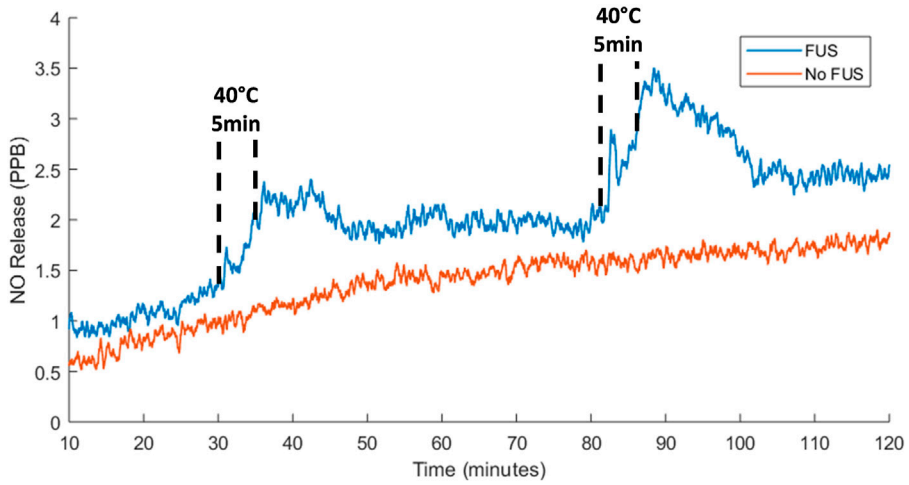

FIGURE 11
Instantaneous NO release from 4.8 mg SF hydrogels with no FUS stimulus and two 40°C FUS heating treatments where hydrogel warming was achieved with a peak acoustic pressure of 5.8 MPa and maintenance at 40°C for 5 min was obtained with a peak acoustic pressure of 3 MPa.

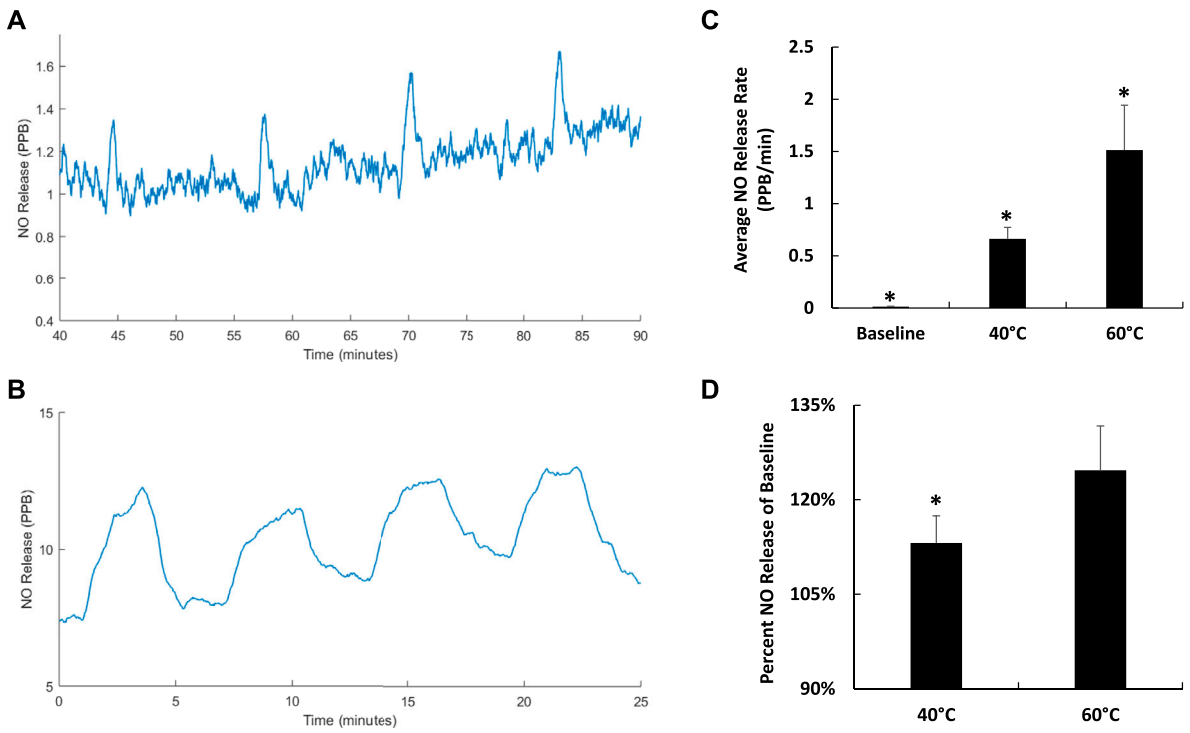

FIGURE 12
Instantaneous NO release from 4.8 mg SF hydrogels with cycles of 40°C **(A)** and 60°C **(B)** FUS heating treatments where hydrogel warming was achieved with a peak acoustic pressure of ±5.8 MPa. Average NO release rate with no FUS treatment and during hydrogel warming cycles to 40°C and 60°C with FUS (n = 4) (*$p < 0.05$) **(C)**. Percent NO release during hydrogel warming cycles to 40°C and 60°C compared to baseline NO release (n = 4) (*$p < 0.05$) **(D)**.

increased the amount and duration of NO peak release (12–13 PPB) during each heating and cooling cycle (Figure 12B). Therefore, altering the magnitude of FUS heating also provides a means of controlling the amount of NO release from hydrogels. Average NO release rates during FUS induced hydrogel warming cycles to 40°C and 60°C were 0.663 ± 0.110 PPB/min and 1.513 ± 0.430 PPB/min respectively (Figure 12C). Both of these FUS induced release rates were

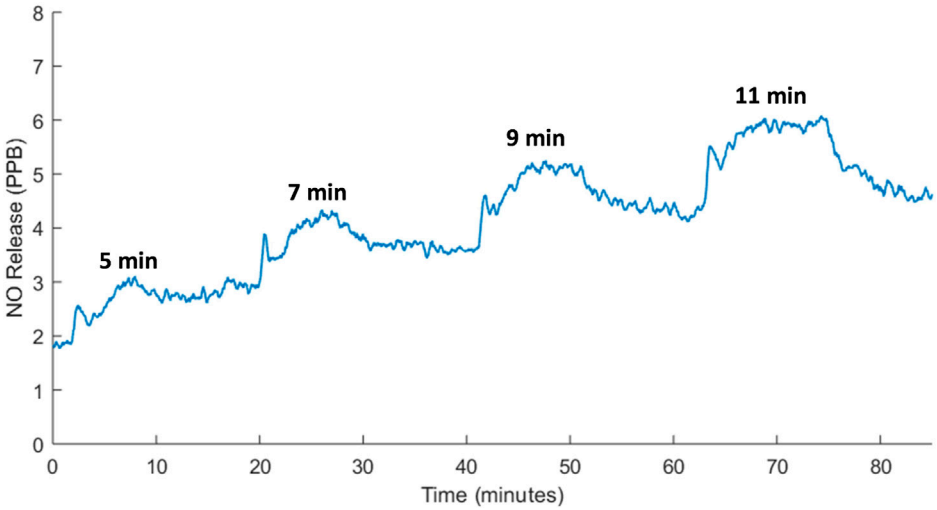

FIGURE 13
Real-time NO release from SF hydrogels with 5–11 min of FUS heating at 40°C and 12-min cooling intervals showing tight temporal control over remote NO delivery. Hydrogel warming was achieved with a peak acoustic pressure of ±5.8 MPa and maintenance at 40°C was obtained with a peak acoustic pressure of ±3 MPa.

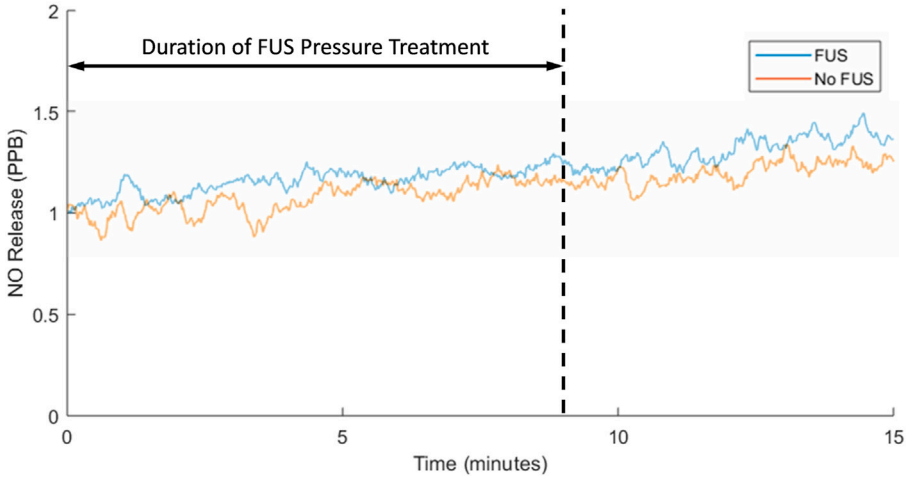

FIGURE 14
NO release from 4.8 mg SNAP-fibrin particles in composite hydrogels treated with FUS pressure stimulus (±3 MPa) at a 10% duty cycle for 9.5 min.

significantly greater than average baseline release of 0.013 ± 0.005 PPB/min. The percent of NO release during hydrogel warming cycles to 40°C and 60°C with FUS were 113% ± 4% and 125% ± 7% of NO baseline release amounts respectively, further demonstrating that FUS thermal stimulus magnitude can controllably elicit NO release from the composite hydrogels (Figure 12D).

To further demonstrate temporal control over NO release with FUS, the duration of FUS heating at 40°C treatment was varied from 5–11 min with 12-min cooling intervals. Results indicated that as the period of heating was increased, heightened NO release was sustained for longer intervals closely matching the duration of 40°C heating (Figure 13). The exact biological relevance of the NO levels elicited from the composite hydrogels for tendon repair applications warrants further study. However, previous literature reports that endogenous presentation and exogenous delivery of NO plays a vital role in collagen synthesis and extracellular matrix regulation in healing tendons (Lin et al., 2001a; Lin et al., 2001b; Murrell, 2007; Murrell et al., 2008; Bokhari and Murrell, 2012).

To evaluate the potential contribution of FUS pressure stimulus to elicit NO release during thermal treatment, pulse width modulation was utilized to isolate temperature (40°C) and pressure (±3 MPa) stimulus. The duty cycle of the FUS driving signal was set to 10% and the duration of treatment was adjusted from 5 to 9.5 min to deliver the same effective pressure dosing

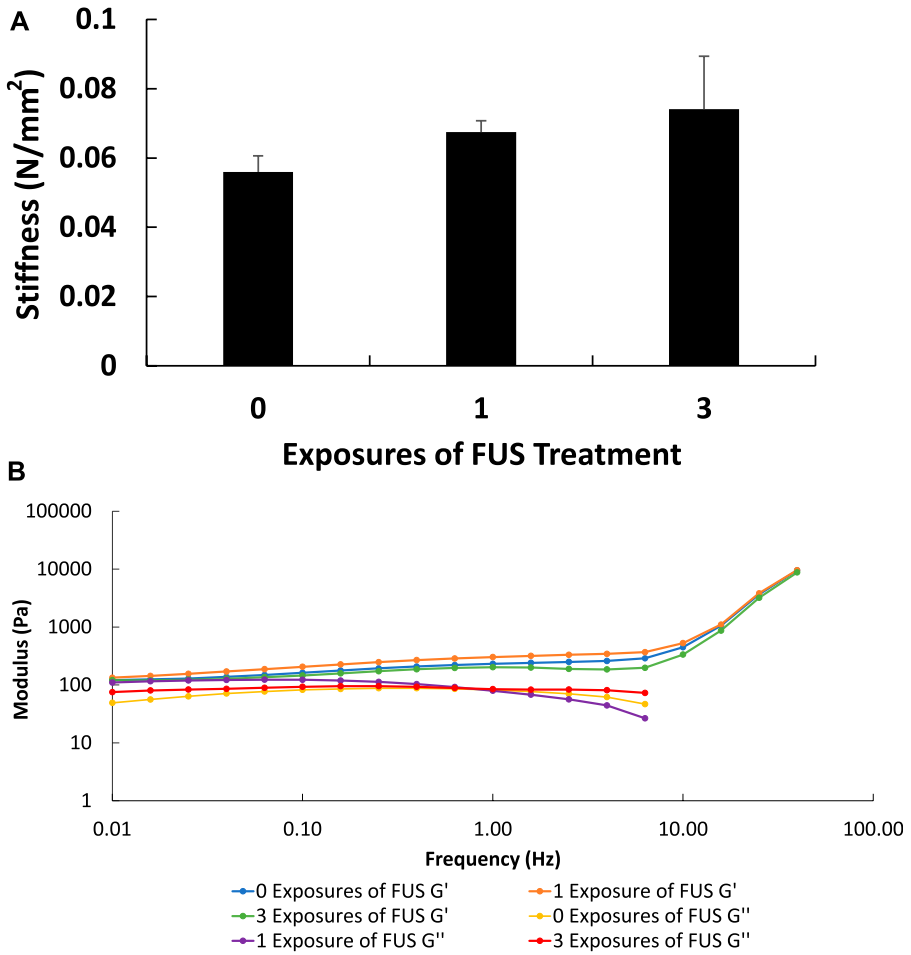

FIGURE 15
Indentation testing showed no significant differences in hydrogel stiffness among samples treated with 0, 1, and 3 exposures of 40°C FUS treatment for 5 min (n = 3) ($p < 0.05$) **(A)**. Representative rheometry results showed that there were no differences in storage and loss modulus measurements among samples treated with 0, 1, and 3 exposures of 40°C FUS treatment for 5 min **(B)**.

(i.e., equivalent FUS pulses) associated with a 100% duty cycle. Composite hydrogels containing 4.8 mg of SNAP-fibrin particles were treated with FUS mechanical stimulus did not show any distinct spikes in NO release, only a gradual increase in NO amount associated with baseline delivery from the hydrogel while a minimal temperature rise (<1°C) over the duration of the treatment was observed (Figure 14). This suggests that FUS thermal stimulus was the major contributor to NO release from hydrogels in this study when compared to the pressures generated during treatment regimens. Future pressure studies will further evaluate the effects of higher FUS generated pressures on NO release from hydrogels.

3.4 Mechanical properties of FUS treated hydrogels

To quantify potential thermal or mechanical damage to hydrogels with FUS treatment, indentation and rheology tests were utilized in the evaluation of bulk hydrogel properties. Composite hydrogels containing 4.8 mg of SNAP-fibrin particles were subject to 0, 1, or 3 exposures of FUS controlled 40°C heating for 5 min. Cavitation was not monitored for during FUS treatment of the hydrogels, but the acoustic parameters used in this study were not known to cause inertial cavitation and no visual differences in FUS treated *versus* untreated hydrogels were observed. Indentation results indicated that there were no significant differences in hydrogel stiffness among samples treated with 0, 1, and 3 exposures of 40°C FUS treatment for 5 min (Figure 15A). Additionally, rheometric characterization further showed that there were no differences in the storage and loss modulus of hydrogels treated with 0, 1, 3, or 5 exposures of FUS controlled 40°C heating for 5 min (Figure 15B). This suggests that FUS did not cause bulk physical damage to the hydrogels for the treatment parameters utilized in this work. Increasing the temperature, pressure, or duration of FUS stimulus may elicit quantifiable damage to hydrogels in future studies. Since only a small, localized volume of hydrogel was treated by FUS, future studies

with volumetric FUS scans of the hydrogels will be completed to further explore the effects of FUS treatment on bulk hydrogel properties.

4 Conclusion

Reactive oxygen species, such as NO, have multiple roles in normal wound healing processes including cell signaling and recruitment (i.e., modulation of phagocyte activation, cell proliferation and apoptosis), regulation of vasculature tone (i.e., vasoconstriction, vasodilation, and promotion of angiogenesis), involvement in innate immunity (i.e., inherent bacteriostatic and bactericidal effects), and the mediation of tissue repair (i.e., transcriptional and post-transcriptional regulation of ECM remodeling enzymes) (Patel et al., 1999; Fang, 2004). This study evaluated the ability of FUS to remotely control the delivery of exogenous NO from injectable composite hydrogels via thermal and mechanical stimulus. Results showed that FUS can controllably heat composite hydrogels to various temperatures over different durations. FEA acoustic simulations also provided visualization of the FUS targeting in the hydrogel. The ability of FUS to modulate the release of NO from SNAP-fibrin μ-particles incorporated in composite hydrogels was verified over various durations and magnitudes of heating. Additionally, pulse width modulation studies suggested that FUS elicits NO release with a dominantly thermal effect. Information gathered in this study will be used towards an ultimate goal of providing a therapeutic approach in accelerating tendon repair through the NO-modulated regulation of ECM synthesis and degradation and prevention of infection by microbial pathogens.

Future work includes determining if FUS can be used to remotely activate and/or inhibit the mechanisms involved in the balance of ECM synthesis and degradation during wound healing via the controlled release of NO *in vitro*. Additionally, other therapeutic molecules and/or donors could be incorporated into fibrin μ-particles to induce the release of various reactive oxygen species (i.e., H_2O_2), growth factors, cytokines, *etc.* The effects of a FUS system on NO release from composite hydrogels with *in vivo* models will also be evaluated as a potential for ablate and replace therapies in clinical settings.

Data availability statement

The raw data supporting the conclusions of this article will be made available by the authors, without undue reservation.

Author contributions

KM and RR developed the methodology for the hydrogel synthesis and characterization experiments. AS, ZK, and EV developed the methodology for focused ultrasound experiments. KM developed and conducted theoretical FUS modelling experiments. KM conducted experiments and gathered the data for all experimental studies. KM led all data analysis with support from AS, ZK, RR, and EV. KM led the writing of the manuscript. All authors contributed critically to drafts of the manuscript and gave final approval for this submission.

Funding

This work was supported in part by grants from the NIH (R15-GM112082 and R15-GM137298) (RR), the Focused Ultrasound Foundation through the Charles Steger Global Internship Program (KM), and the Barry Goldwater Scholarship and Excellence in Education Foundation (KM).

Conflict of interest

The authors declare that the research was conducted in the absence of any commercial or financial relationships that could be construed as a potential conflict of interest.

Publisher's note

All claims expressed in this article are solely those of the authors and do not necessarily represent those of their affiliated organizations, or those of the publisher, the editors and the reviewers. Any product that may be evaluated in this article, or claim that may be made by its manufacturer, is not guaranteed or endorsed by the publisher.

References

Behrouzkia, Z., Joveini, Z., Keshavarzi, B., Eyvazzadeh, N., and Aghdam, R. Z. (2016). Hyperthermia: How can it Be used? *Oman Med. J.* 31 (2), 89–97. doi:10.5001/omj.2016.19

Bogdan, C. (2001). Nitric oxide and the immune response. *Nat. Immunol.* 2 (10), 907–916. doi:10.1038/ni1001-907

Bogdan, C., Rollinghoff, M., and Diefenbach, A. (2000). Reactive oxygen and reactive nitrogen intermediates in innate and specific immunity. *Curr. Opin. Immunol.* 12 (1), 64–76. doi:10.1016/s0952-7915(99)00052-7

Bokhari, A. R., and Murrell, G. A. (2012). The role of nitric oxide in tendon healing. *J. Shoulder Elb. Surg.* 21 (2), 238–244. doi:10.1016/j.jse.2011.11.001

Burgess, M. T., Apostolakis, I., and Konofagou, E. E. (2018). Power cavitation-guided blood-brain barrier opening with focused ultrasound and microbubbles. *Phys. Med. Biol.* 63 (6), 065009. doi:10.1088/1361-6560/aab05c

Cabaleiro, D., Hamze, S., Fal, J., Marcos, M. A., Estellé, P., and Żyła, G. (2020). Thermal and physical characterization of PEG phase change materials enhanced by carbon-based nanoparticles. *Nanomater. (Basel)* 10 (6), 1168. doi:10.3390/nano10061168

Chakrabarti, S., and Patel, K. D. (2005). Matrix metalloproteinase-2 (MMP-2) and MMP-9 in pulmonary pathology. *Exp. Lung Res.* 31 (6), 599–621. doi:10.1080/019021490944232

de Vries, J. J., Snoek, C. J., Rijken, D. C., and de Maat, M. P. (2020). Effects of post-translational modifications of fibrinogen on clot formation, clot structure, and fibrinolysis: A systematic review. *Arterioscler. Thromb. Vasc. Biol.* 40 (3), 554–569. doi:10.1161/atvbaha.119.313626

Drakos, T., Antoniou, A., Evripidou, N., Alecou, T., Giannakou, M., Menikou, G., et al. (2021). Ultrasonic attenuation of an agar, silicon dioxide, and evaporated milk gel phantom. *J. Med. Ultrasound* 29 (4), 239–249. doi:10.4103/JMU.JMU_145_20

Dunnill, C., Patton, T., Brennan, J., Barrett, J., Dryden, M., Cooke, J., et al. (2017). Reactive oxygen species (ROS) and wound healing: The functional role of ROS and emerging ROS-modulating technologies for augmentation of the healing process. *Int. Wound J.* 14 (1), 89–96. doi:10.1111/iwj.12557

Fang, F. C. (2004). Antimicrobial reactive oxygen and nitrogen species: Concepts and controversies. *Nat. Rev. Microbiol.* 2 (10), 820–832. doi:10.1038/nrmicro1004

Focused Ultrasound Induced Heating in Tissue Phantom Focused ultrasound induced heating in tissue phantom. Available at: https://www.comsol.com/model/focused-ultrasound-induced-heating-in-tissue-phantom-12659.

Garcia-Ortiz, A., and Serrador, J. M. (2018). Nitric oxide signaling in T cell-mediated immunity. *Trends Mol. Med.* 24 (4), 412–427. doi:10.1016/j.molmed.2018.02.002

Guzik, T. J., Korbut, R., and Adamek-Guzik, T. (2003). Nitric oxide and superoxide in inflammation and immune regulation. *J. Physiol. Pharmacol.* 54 (4), 469–487.

Halder, G., Dupont, S., and Piccolo, S. (2012). Transduction of mechanical and cytoskeletal cues by YAP and TAZ. *Nat. Rev. Mol. Cell Biol.* 13 (9), 591–600. doi:10.1038/nrm3416

He, W., and Frost, M. C. (2016). CellNO trap: Novel device for quantitative, real-time, direct measurement of nitric oxide from cultured RAW 267.4 macrophages. *Redox Biol.* 8, 383–397. doi:10.1016/j.redox.2016.03.006

He, W., and Frost, M. C. (2016). Direct measurement of actual levels of nitric oxide (NO) in cell culture conditions using soluble NO donors. *Redox Biol.* 9, 1–14. doi:10.1016/j.redox.2016.05.002

Joseph, C. A., McCarthy, C. W., Tyo, A. G., Hubbard, K. R., Fisher, H. C., Altscheffel, J. A., et al. (2019). Development of an injectable nitric oxide releasing poly(ethylene) glycol-fibrin adhesive hydrogel. *ACS Biomaterials Sci. Eng.* 5 (2), 959–969. doi:10.1021/acsbiomaterials.8b01331

Khirallah, J., Schmieley, R., Demirel, E., Rehman, T. U., Howell, J., Durmaz, Y. Y., et al. (2019). Nanoparticle-mediated histotripsy (NMH) using perfluorohexane 'nanocones'. *Phys. Med. Biol.* 64 (12), 125018. doi:10.1088/1361-6560/ab207e

Kim, J. O., Noh, J.-K., Thapa, R. K., Hasan, N., Choi, M., Kim, J. H., et al. (2015). Nitric oxide-releasing chitosan film for enhanced antibacterial and *in vivo* wound-healing efficacy. *Int. J. Biol. Macromol.* 79, 217–225. doi:10.1016/j.ijbiomac.2015.04.073

Lapin, N. A., Gill, K., Shah, B. R., and Chopra, R. (2020). Consistent opening of the blood brain barrier using focused ultrasound with constant intravenous infusion of microbubble agent. *Sci. Rep.* 10 (1), 16546. doi:10.1038/s41598-020-73312-9

Lin, J. H., Wang, M. X., Wei, A., Zhu, W., Diwan, A. D., and Murrell, G. A. C. (2001). Temporal expression of nitric oxide synthase isoforms in healing Achilles tendon. *J. Orthop. Res.* 19 (1), 136–142. doi:10.1016/s0736-0266(00)00019-x

Lin, J., Wang, M. X., Wei, A., Zhu, W., and Murrell, G. A. C. (2001). The cell specific temporal expression of nitric oxide synthase isoforms during achilles tendon healing. *Inflamm. Res.* 50 (10), 515–522. doi:10.1007/pl00000228

Moncion, A., Arlotta, K. J., Kripfgans, O. D., Fowlkes, J. B., Carson, P. L., Putnam, A. J., et al. (2016). Design and characterization of fibrin-based acoustically responsive scaffolds for tissue engineering applications. *Ultrasound Med. Biol.* 42 (1), 257–271. doi:10.1016/j.ultrasmedbio.2015.08.018

Murrell, G. A., Tang, G., Appleyard, R. C., del Soldato, P., and Wang, M. X. (2008). Addition of nitric oxide through nitric oxide-paracetamol enhances healing rat achilles tendon. *Clin. Orthop. Relat. Res.* 466 (7), 1618–1624. doi:10.1007/s11999-008-0271-y

Murrell, G. A. (2007). Using nitric oxide to treat tendinopathy. *Br. J. Sports Med.* 41 (4), 227–231. doi:10.1136/bjsm.2006.034447

Narkar, A. R., Kendrick, C., Bellur, K., Leftwich, T., Zhang, Z., and Lee, B. P. (2019). Rapidly responsive smart adhesive-coated micropillars utilizing catechol-boronate complexation chemistry. *Soft Matter* 15 (27), 5474–5482. doi:10.1039/c9sm00649d

Nourissat, G., Berenbaum, F., and Duprez, D. (2015). Tendon injury: From biology to tendon repair. *Nat. Rev. Rheumatol.* 11 (4), 223–233. doi:10.1038/nrrheum.2015.26

Patel, R. P., McAndrew, J., Sellak, H., White, C., Jo, H., Freeman, B. A., et al. (1999). Biological aspects of reactive nitrogen species. *Biochim. Biophys. Acta* 1411 (2-3), 385–400. doi:10.1016/s0005-2728(99)00028-6

Pitt, W. G., Husseini, G. A., and Staples, B. J. (2004). Ultrasonic drug delivery-a general review. *Expert Opin. Drug Deliv.* 1 (1), 37–56. doi:10.1517/17425247.1.1.37

Rao, W., Deng, Z. S., and Liu, J. (2010). A review of hyperthermia combined with radiotherapy/chemotherapy on malignant tumors. *Crit. Rev. Biomed. Eng.* 38 (1), 101–116. doi:10.1615/critrevbiomedeng.v38.i1.80

Rehman, T. U., Khirallah, J., Demirel, E., Howell, J., Vlaisavljevich, E., and Yuksel Durmaz, Y. (2019). Development of acoustically active nanocones using the host-guest interaction as a new histotripsy agent. *ACS Omega* 4 (2), 4176–4184. doi:10.1021/acsomega.8b02922

Rice, M. A., Waters, K. R., and Anseth, K. S. (2009). Ultrasound monitoring of cartilaginous matrix evolution in degradable PEG hydrogels. *Acta Biomater.* 5 (1), 152–161. doi:10.1016/j.actbio.2008.07.036

Schildkopf, P., J. Ott, O., Frey, B., Wadepohl, M., Sauer, R., Fietkau, R., et al. (2010). Biological rationales and clinical applications of temperature controlled hyperthermia-implications for multimodal cancer treatments. *Curr. Med. Chem.* 17 (27), 3045–3057. doi:10.2174/092986710791959774

ter Haar, G. (2015). Heat and sound: Focused ultrasound in the clinic. *Int. J. Hyperth.* 31 (3), 223–224. doi:10.3109/02656736.2015.1014434

Trappmann, B., Gautrot, J. E., Connelly, J. T., Strange, D. G. T., Li, Y., Oyen, M. L., et al. (2012). Extracellular-matrix tethering regulates stem-cell fate. *Nat. Mater* 11 (7), 642–649. doi:10.1038/nmat3339

VanWagner, M., Rhadigan, J., Lancina, M., Lebovsky, A., Romanowicz, G., Holmes, H., et al. (2013). S-nitroso-N-acetylpenicillamine (SNAP) derivatization of peptide primary amines to create inducible nitric oxide donor biomaterials. *ACS Appl. Mater. interfaces* 5 (17), 8430–8439. doi:10.1021/am4017945

Vogel, V., and Sheetz, M. (2006). Local force and geometry sensing regulate cell functions. *Nat. Rev. Mol. Cell Biol.* 7 (4), 265–275. doi:10.1038/nrm1890

Watt, F. M., and Hogan, B. L. (2000). Out of eden: Stem cells and their niches. *Science* 287 (5457), 1427–1430. doi:10.1126/science.287.5457.1427

Yildirim, A., Blum, N. T., and Goodwin, A. P. (2019). Colloids, nanoparticles, and materials for imaging, delivery, ablation, and theranostics by focused ultrasound (FUS). *Theranostics* 9 (9), 2572–2594. doi:10.7150/thno.32424

Zhou, Y. F. (2011). High intensity focused ultrasound in clinical tumor ablation. *World J. Clin. Oncol.* 2 (1), 8–27. doi:10.5306/wjco.v2.i1.8